Edit Trace of Manuscript 10.1021/acs.jpcc.7b05090

Detailed Investigation of Thermal Regeneration of High-~~silica~~Silica ZSM-5 Zeolite through *in ~~situ~~Situ* Synchrotron X-ray Powder Diffraction and Adsorption Studies

Author, please respond to the following questions:

Author: The graphic for the TOC/Abstract is somewhat low resolution. If you would like to provide a new graphic with a higher resolution, then please provide a revised graphic with your galley corrections..... 2

Elisa **Rodeghero** ,~~a†*~~a† ■ Annalisa **Martucci** ,a† ■ Giuseppe **Cruciani** ,a† ■ Elena **Sarti** ,b‡ ■ Alberto **Cavazzini** ,b‡ ■ Valentina **Costa** ,b‡ ■ Roberto **Bagatin** ,c§ ■ **and** Luisa **Pasti** ~~b‡~~*b‡ ■ ■

~~a†~~ **Department of Physics and Earth Sciences** ~~Department of Physics and Earth Sciences,~~ **University of Ferrara**■ , Via Saragat 1, I-44123 Ferrara ~~(FE),~~ Italy ~~.~~

~~b‡~~ **Department of Chemistry and Pharmaceutical Sciences**, **University of Ferrara** , Via L. Borsari 46, I-44121 Ferrara ~~(FE),~~ Italy

~~c§~~ **Research Center for Non-Conventional Energy** ~~Research Center, for Non-Conventional Energy —~~ **Istituto Eni Donegani Environmental Technologies** , via Maritano~~,~~ 26, San Donato Milanese ~~(MI),~~ Milan I-20097, Italy ~~.~~

* ~~Corresponding Authors~~E~~e~~-mail: rdglse@unife.it .

** ~~e~~E-mail: psu@unife.it .

Adsorption is important for many applications including catalysis and water remediation technology. To improve the performances of such applications, it is essential to have a deep understanding of adsorbent ~~–~~–adsorbate interactions, and of the dynamics involved in adsorption/desorption processes of porous adsorbent materials. In this study, the thermal desorption of high-silica (HS) ZSM-5 zeolite loaded with mixtures of organic compounds (namely, methyl *tert*-butyl ether/toluene, and methyl *tert*-butyl ether/1,2 dichloroethane) was investigated in real time using *in situ* high-temperature synchrotron X-ray powder diffraction (HT-XRPD). A picture of both kinetics and dynamic behavior of this adsorbent during thermal regeneration is presented, including the evolution of refined occupancies of the host molecules as a function of temperature. The adsorption enthalpy and entropy of the organic compound were also evaluated and compared with desorption temperature. It was found that configurational effects can affect the mobility of the molecules inside the framework, and~~,~~ in particular, the desorption temperature seems to be mainly related to the position of the molecule inside the porous structure.

Author: The graphic for the TOC/Abstract is somewhat low resolution. If you would like to provide a new graphic with a higher resolution, then please provide a revised graphic with your galley corrections.

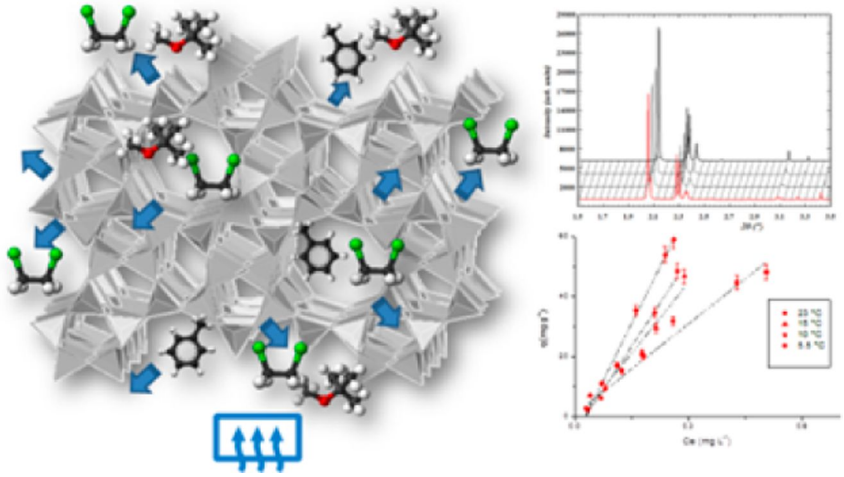

Abstract Graphic

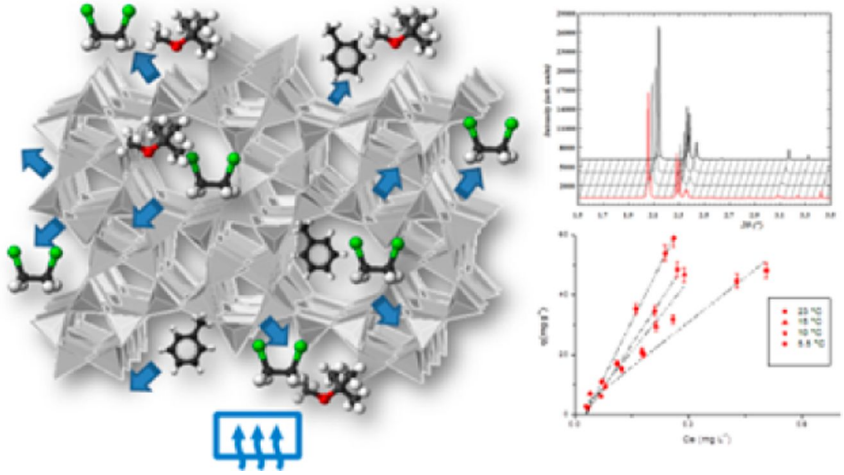

TOC Graphic

SI File: jp7b05090_si_001.pdf

1. Introduction

Zeolites are crystalline, microporous materials characterized by high porosity and large surface area. The well-defined pore structure confers on them the ability to host atoms or molecules inside cages or channels delimited by the framework as well as ~~controls~~to control the concentration and thermodynamic state of sorbed molecules. [1−11] Moreover, affinity ~~towards~~toward organic species may be appropriately tuned by varying the SiO_2/Al_2O_3 ratio (SAR) and, consequently, the hydrophobicity of these materials. The combination of steric hindrance and chemical interactions inside the zeolitic pore system in combination with their excellent thermal and chemical stability makes these materials suitable for many applications including adsorption. [12−17] Indeed, it has been recently highlighted that high -silica (HS) zeolites such as zeolite beta (BEA), mordenite (MOR), ferrierite (FER), Y (FAU), and ZSM-5 (MFI) exhibit good properties for fuel-based compounds adsorption from aqueous solutions. [14−26] Additionally, as adsorbents, zeolites can be easily regenerated by several methods including solvent extraction, microwave and ultrasounds, photochemical, biological, vacuum, electrochemical, and thermal treatments [27−29] in the latter case, the full recyclability of the sorbent has been also demonstrated. [18,20]

Zeolites with MFI topology have been extensively studied, due their interesting pore system, which define three different sorption sites: straight channel (SC), sinusoidal channel (ZZ) and intersection. [30–31] In particular, in ~~Ref.~~ref 17 the adsorption of methyl *tert*-butyl ether (MTBE)/toluene (TOL~~),~~ and 1,2 dichloroethane (DCE) /MTBE binary mixtures in aqueous solution on ZSM-5 has been described by a competitive model, namely, a dual site Langmuir adsorption isotherm. Rietveld structure refinements provided information about the relative position of the MTBE-TOL and MTBE-DCE mixtures inside the porous structure of ZSM-5 ~~as well as they~~and clearly highlighted the structural interactions between the zeolite lattice and sorbate molecules. It has been found that MTBE and DCE molecules (ZSM-5-MTBE-DCE sample) are located in two independent ~~extraframework~~extra-framework sites: MTBE is hosted near the SC channel (MTBE1 site, see Figure 1 a), whereas DCE is in the ZZ channel (DCE2 site, Figure 1 a). ~~On the other hand~~However, in ZSM-5-MTBE-TOL, TOL and MTBE molecules are confined near the SC (TOL1 site) and ZZ channels (MTBE2 site), respectively[17] (see Figure 1 b). These results suggested that MTBE can occupy different positions in the ZSM-5 porous system, depending on the composition of the investigated mixture.

Figure 1. Unit cells with the modeled atoms of (a) ZSM-5-MTBE-DCE~~,~~ and (b) ZSM-5-MTBE-TOL ~~adsorbed~~. Adsorbed molecules along *a* and *b* directions, respectively.

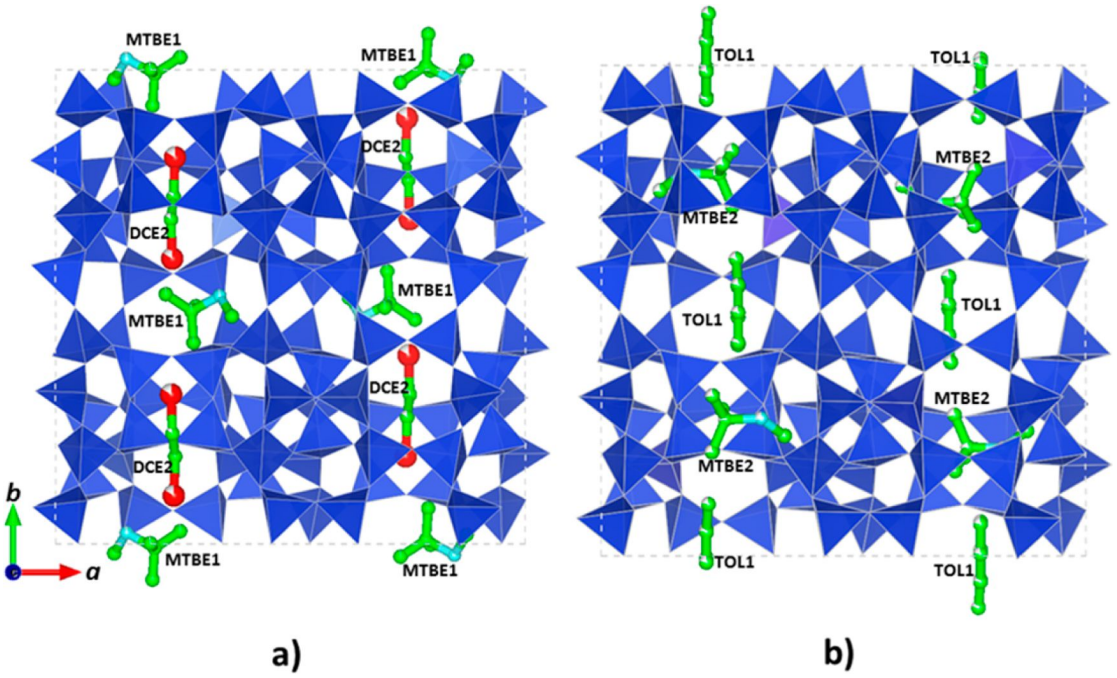

In this study, we provide detailed information on the thermal desorption behavior of high -silica ZSM-5 zeolite loaded with MTBE-DCE and DCE-TOL binary mixtures. *In situ* high-temperature synchrotron X-ray powder diffraction (HT-XRPD) has allowed to ~~continuously~~continuous monitoring of the dynamic ~~behaviour~~behavior of ZSM-5-loaded structures. This study has also involved the analysis of the occupancies of the host molecules inside the zeolitic framework during the temperature-induced desorption process. Finally, the thermodynamics of adsorption (from aqueous solutions) ~~has~~have also been investigated in order to compare the order of release of organic compounds with their adsorption enthalpy. Indeed, the ultimate scope of this work has been to investigate whether temperature -induced desorption correlates to traditional thermodynamic parameters, such as the adsorption enthalpy of adsorbed molecules, or ~~instead~~ if instead other effects of kinetic nature should be considered (e.g., steric hindrance, constrained diffusion in the zeolite framework, etc.). To the best of our knowledge, this is the first example of this kind of investigation.

The outcome of this research could be useful to fine-tune industrially relevant adsorption and separation processes. Indeed, the design and development of many emerging separation and catalytic process technologies require a proper quantitative description of diffusion of mixtures of guest molecules within microporous structures. [32–34] Consequently,

they are relevant both for zeolite characterization and application, because the response to heating of microporous crystalline materials can vary dramatically not only from one material to another but also depending can depend on the nature and concentrations of embedded species. [35–37]

2. Experimental Section

2.1. Materials

The ZSM-5 sample used in this work was a hydrophobic zeolite (code CBV 28014) provided by Zeolyst International in its ammonium form (NH_4^+ content was lower than 1% wt %) and used as received. The manufacturer of the CBV 28014 zeolite reports a SiO_2/Al_2O_3 molar ratio equal to 280, a Na_2O content lower than 0.05 wt.%, and a surface area of 400 $m^2\ g^{-1}$.

2.2. Batch experiments Experiments

Adsorption isotherms were determined through batch method. Batch experiments were carried out in duplicate in 20 ml mL crimp top reaction glass flasks sealed with PTFE septa (Supelco, PA, USA). The flasks were filled in order to have the minimum headspace. A solid/solution ratio of 1:4 (mg mL^{-1}) was employed. The samples were equilibrated for 24 hoursh at different temperatures (5, 10, 15, and 22.5 °C). During the adsorption, temperature was controlled (± 0.5 °C) by means of a jacketed glass beaker, and a temperature controller was used to circulate water through the reactor jackets (Lab Companion RW-0525G). The samples were kept under stirring by a 10-place magnetic stirrer (IKAMAG RO 10 power, IKA, Stanfer, Germany) at a stirring speed of 500 rpm. After equilibration, the solids were separated from the aqueous solution using centrifugation (14000 14000 rpm for 30 min). To determine both adsorbed quantities (q) and equilibrium concentrations (C_e), TOL, MTBE, and DCE were determined in solutions before and after equilibration with the zeolite. All experiments were carried out in duplicates duplicate (deviations were within 5%).

2.3. Gas Chromatography

The concentration of contaminants in the aqueous solution was determined by Headspace Gas Chromatography coupled to Mass Spectrometry (Hs-GC-MS). The analysis was carried out using an Agilent GC-MS system (Santa Clara, CA, USA) consisting of a GC 6850 Series II Network coupled to a Pal G6500-CTC injector and a Mass Selective Detector 5973 Network.

Hs autosampler injector conditions are as follows: incubation oven temperature 80 °C, incubation time 50 min, headspace syringe temperature 85 °C, agitation speed 250 rpm, agitation on time 30 s, agitation off time 5 s, injection volume 500 µL µL, fill speed 30 µL µL s^{-1}, syringe pull-up delay 5 s, injection speed 250 µL µL s^{-1}, pre-injection preinjection delay 0 s, post injection delay 2 s, and syringe flush 30 s with nitrogen.

A DB-624 UI GC column (L = 20 m, I.D. = 0.18 mm, d_f = 1.00 µm µm film thickness, Agilent, Santa Clara, CA, USA) was used. High -purity helium was the carrier gas with a constant flow rate of 0.7 mL min^{-1}. The oven temperature gradient started at 40 °C for 4 minutes min and was then ramped to 130 °C at 15 °C min^{-1}. The injector temperature was kept at 150 °C. All samples were injected in split mode (10:1).

The mass spectrometer operated in electron impact mode (positive ion, 70 eV). The source temperature and the quadrupole temperature were set to 230 °C and 150 °C respectively.

The mass spectra were acquired in full scan mode. The electronic scan speed was 1562 amu s^{-1} in a mass range from 30 to 300 amu. For identification and quantification of the target analyte the, SIM (selected ion monitoring) chromatograms were extracted from the acquired signal by selecting the most abundant characteristic fragments at m/z = 62.49 (DCE), m/z = 73.57 (MTBE) and m/z= 91.92 (TOL). The Chromatographic peak of analytes was identified by comparison of the retention time and the mass spectrum with standard compound and library data; quantitative analysis was performed using calibration curves.

2.4. Thermal analyses Analyses

Thermogravimetric (TG) and derivative thermogravimetry (DTG) measurements of zeolite samples after mixtures adsorption were performed in air using an STA 409 PC LUXX® Netzsch operating at 10 °C min^{-1} heating rate, from room temperature (RT) to 900 °C.

2.5. Time-resolved diffraction methods Resolved Diffraction Methods and refinement strategy Refinement Strategy

In this work the, *in situ* high -temperature X-ray diffraction is used in order to follow pollutants mixtures release/decomposition process as well as the structural modifications undergoing on ZSM-5 during the thermal treatment. With this purpose, ZSM-5 powders loaded with MTBE-DCE and MTBE-TOL mixtures have been studied with time-- -resolved diffraction technique on the ID22 beamline at ESRF (Grenoble), using a fixed wavelength of 0.400031(1) Å Å and an X-ray transfocator with compound refractive lenses. Using this technique, the presence of the third harmonic has been reduced as well as the suppression of all higher-order harmonics to five 5 orders of magnitude using

monochromator detuning.[38] The data were collected in the 30° – 600–600 °C temperature range. Diffracted X-rays were directed through nine Si(111) analyseranalyzer crystals (channels separated by ≈~2°) and then scanned in a continuous mode, thus registering high-resolution diffraction patterns in parallel. X-ray diffraction patterns were recorded in the 0.5––19.5 2θ range. The automatic indexing of the peaks, performed by means of the HighScore Plus v.3.0 software[39],[39] revealed the monoclinic *P2*2*P* 2_1 *1/n* symmetry.

Table 1. Refinement detailsDetails of the data collectionData Collection and unit cell parametersUnit Cell Parameters of ZSM-5 and ZSM-5 loadedLoaded with binary mixturesBinary Mixtures of MTBE, DCE, and TOL at 30, 100, and 400°C.

	KZSM-5T ZSM-5	KZSM-5-MTBE-DCET ZSM-5-MTBE-DCE			KZSM-5-MTBE-TOLT ZSM-5-MTBE-TOL		
	K30 °Cad T 30°Cad	K30 °Cbe T 30°Cbe	K100 °CT 100°C	K400 °CT 400°C	K30 °Cbe T 30°Cbe	K100 °CT 100°C	K400 °CT 400°C
Space Groupspace group	K $P2_1/n$ T P2 $_1$/n	K $P2_1/n$ T P2 $_1$/n	*P n m a*Pnma	*P n m a*Pnma	K $P2_1/n$ T P2 $_1$/n	*P n m a*Pnma	*P n m a*Pnma
K *a* (Å)T a (Å)	19.900K19.900(1)T (1)	19.900K19.900(1)T (1)	19.936K19.936(1)T (1)	19.926K19.926(1)T (1)	19.895K19.895(1)T (1)	19.932K19.932(1)T (1)	19.919K19.919(1)T (1)
K *b* (Å)T b (Å)	20.117K20.117(1)T (1)	20.116K20.116(1)T (1)	20.115K20.115(1)T (1)	20.087K20.087(1)T (1)	20.114K20.114(1)T (1)	20.114K20.114(1)T (1)	20.081K20.081(1)T (1)
K *c* (Å)T c (Å)	13.389K13.389(1)T (1)	13.387K13.387(1)T (1)	13.409K13.409(1)T (1)	13.396K13.396(1)T (1)	13.383K13.383(1)T (1)	13.405K13.405(1)T (1)	13.393K13.393(1)T (1)
Kβ (deg)T β (°)	90.55K90.55(1)T (1)	90.6K90.6(1)T (1)	90	90	90.59K90.59(1)T (1)	90	90
K *V* (Å³)T V (Å ³)	5359.9K5359.9(3)T (3)	5358.6K5358.6(1)T (1)	5377.4K5377.4(1)T (1)	5361.9K9(1)T (1)	5355.2K5355.2(1)T (1)	5374.1K5374.1(1)T (1)	5357.2K5357.2(1)T (1)
wavelength (ÅÅ)	1.5417K1.5417(1)T (1)	0.400031K0.400031(1)T (1)	0.400031K0.400031(1)T (1)	0.400031K0.400031(1)T (1)	0.400031K0.400031(1)T (1)	0.400031K0.400031(1)T (1)	0.400031K0.400031(1)T (1)
refined pattern 2θ range (°deg)	3K3–110T 110	1K1–24T 24	0.5K0.5–19.5T 19.5	0.5K0.5–19.5T 19.5	1K1–24T 24	0.5K0.5–19.5T 19.5	0.1K0.1–24.5T 24.5
d_{hkl} lattice spacing (ÅÅ)	14.73K14.73–0.82T 0.82	11.46K11.46–0.49T 0.49	22.92K22.92–0.60T 0.60	22.92K22.92–0.60T 0.60	11.46K11.46–0.49T 0.49	22.92K22.92–0.60T 0.60	114.60K114.60–0.48T 0.48
K R_{wp} (%)a T R wp (%)	9.12	12.4	13.2	13.9	15.4	18	14.5
K R_p (%)b T R p (%)	8.4	9.2	9.9	10.3	11.04	13.7	11.2
K R_{F^2} (%)c T R F 2 (%)	9.1	8.8	8.2	8.4	9	11.8	10.7
no. of contributing reflections	14142	11760	9397	9397	11783	9392	11899
N_{obs}	5601	6357	1892	1888	6477	1828	3559

	ZSM-5	ZSM-5-MTBE-DCE			ZSM-5-MTBE-TOL		
	30 °C[ad]	30 °C[be]	100 °C	400 °C	30 °C[be]	100 °C	400 °C
N_{var}	289	356	208	210	359	209	176
	$R_p = \sum[Y_{io} - Y_{ic}]/\sum Y_{io}$;	$R_{wp} = [\sum w_i (Y_{io} - Y_{ic})^2/\sum w_i Y_{io}^2]^{0.5}$;			$R_{F^2} = \sum\lvert F_o^2 - F_c^2\rvert/\sum\lvert F_o^2\rvert$		

[a] $R_{wp} = [\sum w_i (Y_{io} - Y_{ic})^2/\sum w_i Y_{io}^2]^{0.5}$.

[b] $R_p = \sum[Y_{io} - Y_{ic}]/\sum Y_{io}$.

[c] $R_{F^2} = \sum|F_o^2 - F_c^2|/\sum|F_o^2|$.

[ad] Ref. 25.

[be] Ref. 17.

The GSAS[40] package with the EXPGUI graphical interface[41] was used for Rietveld structure refinements starting from the framework fractional atomic coordinates reported by Pasti et al.[17] Difference Fourier maps, calculated for both ZSM-5-MTBE-DCE and ZSM-5-MTBE-TOL samples, indicates the occurrence of extra-framework sites hosting organic and coadsorbed water molecules. The scale factor was allowed to vary for all histograms. In the final cycles, the refined structural parameters for each data histogram were as follows: fractional coordinates for all atoms, occupancy factors for extra-framework organics and water oxygen atoms, and thermal isotropic displacement factors. Soft constraints were imposed on Si–O and O–O framework (1.60 and 2.60 Å, respectively), distances with tolerance values (σ) of 0.04 ÅÅ), and then released after the initial stages of refinement. Furthermore, the displacement parameters for a given atom type were constrained to be equivalent (i.e., Si and O sites), in order to reduce the number of refined atomic displacement parameters. The refinement of the atomic coordinates, the atomic site occupancies for extra-framework positions, and the isotropic thermal parameters has been performed with the aid of soft constraints (with an initial weight of 10000) on the bond lengths, used as additional observations in the earlier stages of the refinement and progressively reduced to zero.[42] The Bragg peak shape was modeled using a modified pseudo-Voigt function[43] with 0.01% cutoff peak intensity. The instrumental background was empirically fitted using a Chebyschev polynomial of the first kind with 16 variable coefficients for room temperature and 24 variable coefficients for high-temperature data set. The evolution of unit cell parameters as a function of temperature are reported in Figure 2 a and b for the system ZSM-5-MTBE-TOL and ZSM-5-MTBE-DCE, respectively. Table 1 summarizes the refinement details[40] of three selected patterns, collected at 30, 100, and 400 °C, respectively, for comparison the refinement details of ZSM-5 at 30 °C are also reported. The refined atomic coordinates, occupancy factors, and thermal parameters for the corresponding structures at these temperatures are given as Tables S1–S6. The evolution of the thermal isotropic displacement factors for framework T and O atoms in ZSM-5-MTBE-DCE and ZSM-5-MTBE-TOL systems is reported in Figures S1 and S2.

3. Results and Discussion

3.1. Temperature-Dependent Variation of Cell Parameters and Crystal Structure Modifications upon Mixtures Desorption

The results of our Rietveld refinement of ZSM-5-MTBE-TOL and ZSM-5-MTBE-DCE crystal structures at room temperature are in close agreement to what recently reported by Pasti et al.[17] The parameters of the *P2P* 2_1 *//n* cell at room temperature are a_0 = 19.900(1) ÅÅ, b_0 = 20.116(1) ÅÅ, c_0 = 13.387(1) ÅÅ, β = 90.6(1), V_0 = 5358.6(1) ÅÅ^3 in ZSM-5-MTBE-DCE and a_0 = 19.895(1) ÅÅ, b_0 = 20.114(1) ÅÅ, c_0 = 13.383(1), β = 90.59°(1), V_0 = 5355.2(1) ÅÅ^3 in ZSM-5-MTBE-TOL, respectively. The extra-framework refined occupancies confirmed that organics (~3.8 TOL and 3.4 MTBE molecules per unit cell (p.c.u.) in ZSM-5-MTBE-TOL; ~3MTBE3 MTBE and 2.5 DCE in ZSM-5-MTBE-DCE p.c.u.) interact with coadsorbed water molecules thus forming organic–water complexes (clusters or short chains) interacting with the framework oxygens.

Figure 2. Temperature evolution of (a) ZSM-5-MTBE-DCE and (b) ZSM-5-MTBE-TOL, unit cell parameters during *in situ* thermal organic desorption. All values are normalized compared to those refined at room temperature. Errors are smaller than symbols.

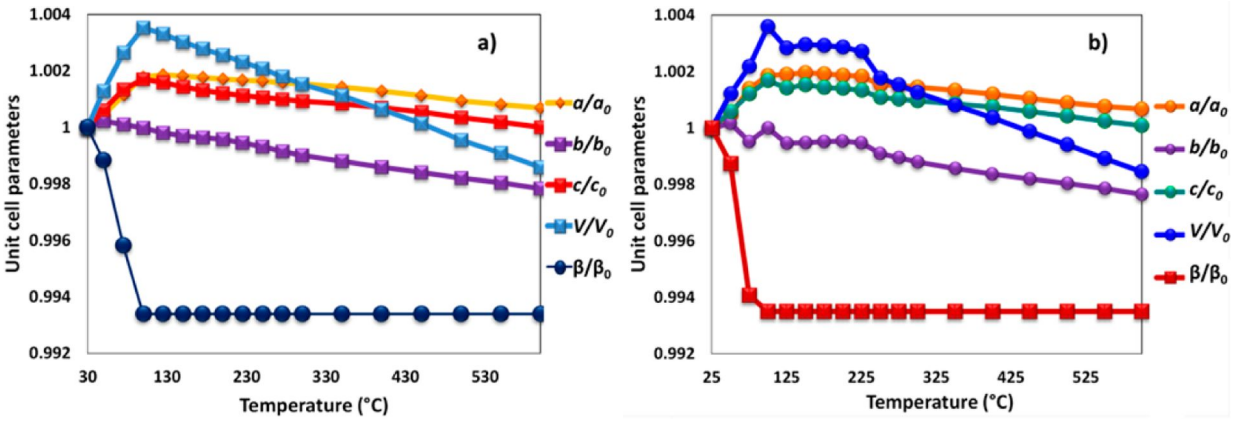

A careful examination of the unit cell parameters plotted in Figures 2 a and 2b as normalized values, $a(T)/a_0$, $b(T)/b_0$, $c(T)/c_0$, and $V(T)/V_0$ revealed that after heating up to 100 °C a slight increase in the unit-cell volume is observed in both samples. At the same time, no changes are observed in ~~extraframework~~extra-framework site occupancies reported in ~~Figures~~Figure 3 a ~~and~~ ,b, indicating that this transient framework expansion is mainly related to the release of host––guest interactions.

Figure 3. Evolution of the number of host molecules per unit cell as a function of temperature in: (a) ZSM-5-MTBE-TOL, and (b) ZSM-5-MTBE-DCE. Errors are smaller than symbols.

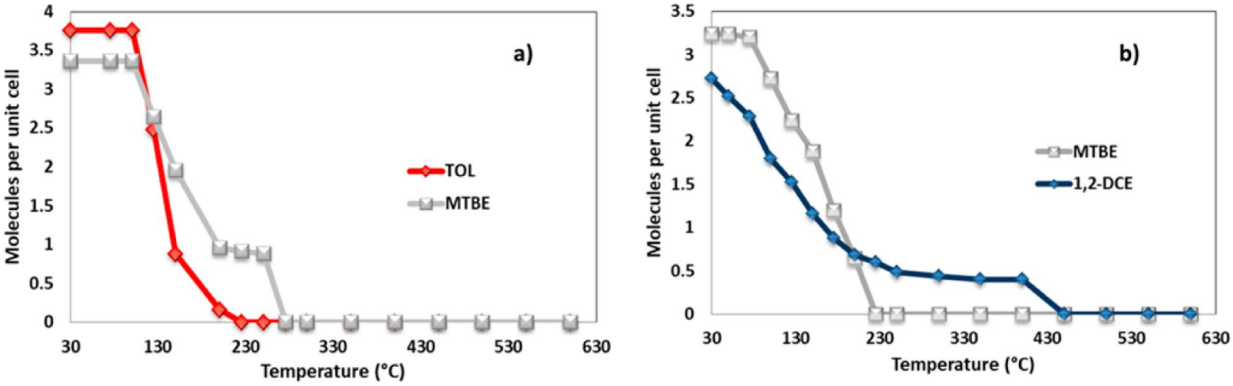

The weakening of hydrogen bonding network is well -known in the zeolite frameworks during the initial heating stages (e.g., in hydro-sodalite[44] ,[44] ~~in~~analcime,[45] ~~analcime~~wairakite[45] ,[46] ~~in wairakite~~[46] , ~~in~~ silica sodalite,[47] cavansite,[48] ~~; in~~ ZSM-5-toluene,[18] and DCE-loaded[20] ,[20] and in the same as-synthesized-high silica-ZSM-5[49] used in this work) ~~and~~; recently, it was described by Martucci et al.[48] as a "pore-mouth-breathing motion". This breathing is associated ~~to~~with a transient slight opening and regularization of the pore apertures, which is followed by a contraction. Upon 100 °C the gradual overlapping of groups of peaks reveals the monoclinic ~~*P2P*~~ 2_1 ~~*1/n*~~ to orthorhombic *Pnma* phase transition (see ~~Figures~~Figure 4 a ~~and~~ ,~~4~~ b, for ZSM-5-MTBE-DCE, and ~~Figures~~Figure 4 c ~~and~~ ,d for ZSM-5-MTBE-TOL) which was already recently observed in the same unloaded ZSM-5 before[49] ~~49~~ and after loading with toluene[18] ,[18] 1,2 dichlorethane,[20] and methyl-*tert*-butyl-ether[19] .[19]

Figure 4. Evolution of powder diffraction patterns in the 25––100 °C temperature range: (a) ZSM-5-MTBE-DCE spectra (for the range of 1.7––3.5° 2θ), (b) ZSM-5- MTBE-DCE spectra (for the range of 5.5––7.9° 2θ), (c) ZSM-5-MTBE-TOL spectra (for the range of 1.7––3.5° 2θ), and (d) ZSM-5-MTBE-TOL spectra (for the range of 5.5––7.9° 2θ).

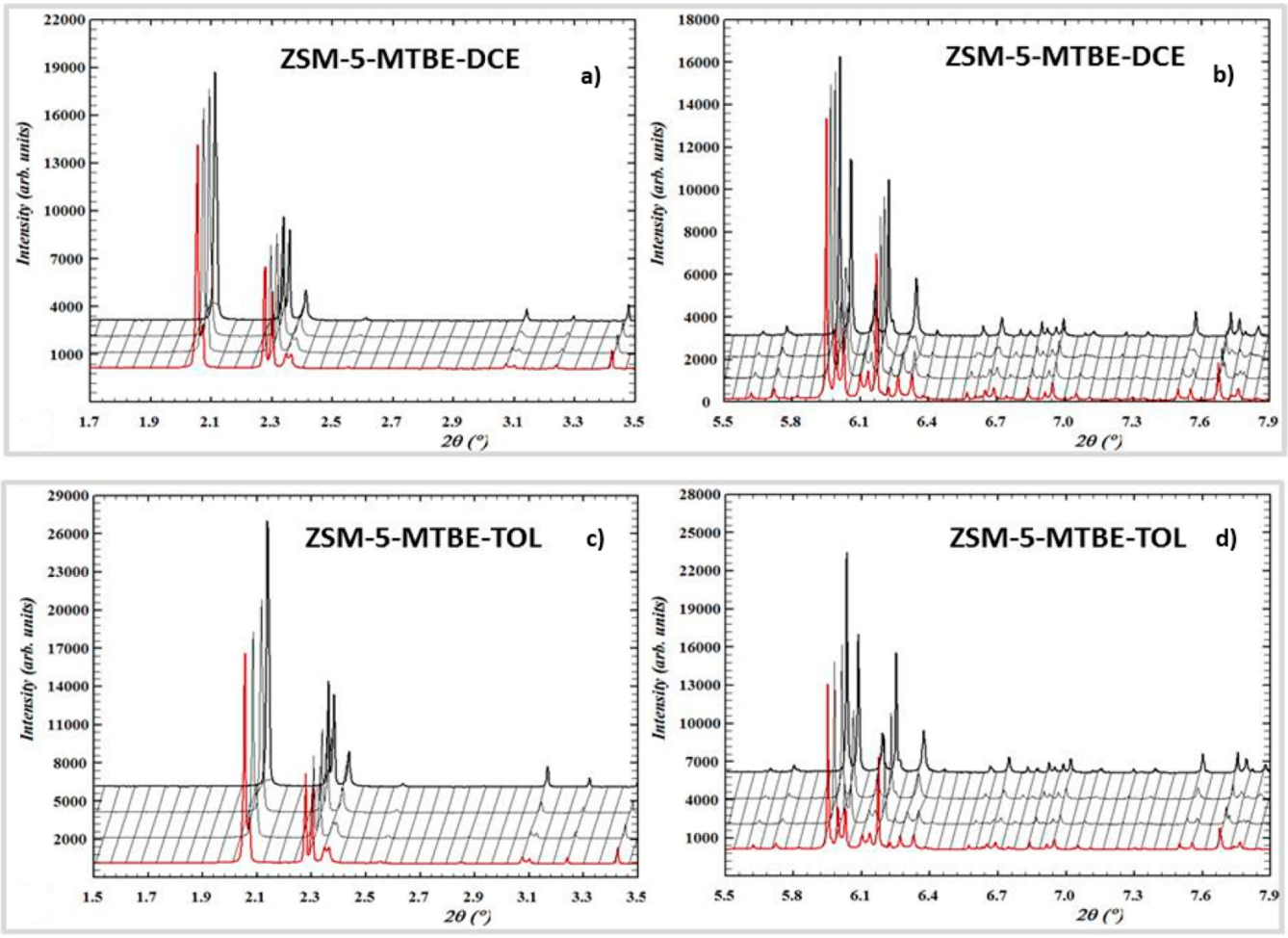

After the phase transition, the unit cell volume decreases and the release/decomposition of the host organic molecules occurs (see Figure 2). Further insights on the sequence of the organics molecules release, can be gained by following the refined occupancies of the TOL, DCE and MTBE sites as a function of temperature plotted in Figure 3 . The release/decomposition of TOL and MTBE starts at about 100 °C and continuously proceeds up to ~250 °C (see Figure 3 a~~),~~; beyond this temperature the sites are completely emptied. The onset of both MTBE and DCE loss from the adsorbent (also occurs at ~100 °C and these sites are fully emptied above 350 °C (see Figure 3 b). The evolution of refined occupancies versus temperature suggests that species hosted in the ZZ or at the channel intersections~~,~~ move more slowly than those adsorbed in or near SC~~,~~ in very good agreement with experimental adsorption enthalpy measured through batch experiments (*vide infra*). As far as concerns water molecules, they are completely released from the cavities at ~500 °C. Thus, based on the ~~extraframework~~extra-framework site occupancy refinements, the *T*-dependent distortion mechanism in the framework takes place in correspondence with guest organic molecule release. Table 2 reports the ~~Crystallographic Free Area~~crystallographic free area (CFA) of both ZZ and SC channels, as well as the ellypticity (ε) of the apertures at 30, 100, and 400 °C temperatures, respectively.

Table 2. Dimensions of the ~~apertures~~Apertures (~~Å~~Å) of ZSM-5 ~~unload~~Unloaded ~~a~~ and after ~~mixtures adsorption~~Mixtures Adsorption of DCE, TOL, and MTBE ~~molecules~~Molecules at 30, 100 and 400°C~~.~~ ~~a~~

Straightstraight channel (K(SC-A)T SC-A)	ε	CFA	Sinu-soidalsinusoidal channel (K(ZZ-A)T ZZ-A)	ε	CFA
ZSMKZSM-5a T 5 a	1.03	22.68	ZSMKZSM-5a T 5 a	1.04	21.65
ZSMKZSM-5-MTBE-DCE-30 °Cb T 5-MTBE-DCE-30°C b	1.07	24.16	ZSMKZSM-5-MTBE-DCE-30 °Cb T 5-MTBE-DCE-30°C b	1.05	24.28
ZSMKZSM-5-MTBE-DCE-100 °CT 5-MTBE-DCE-100°C	1.09	23.84	ZSMKZSM-5-MTBE-DCE-100 °CT 5-MTBE-DCE-100°C	1.04	24.06
ZSMKZSM-5-MTBE-DCE-400 °CT 5-MTBE-DCE-400°C	1.08	23.72	ZSMKZSM-5-MTBE-DCE-400 °CT 5-MTBE-DCE-400°C	1.04	24.13
ZSMKZSM-5-MTBE-TOL-30 °Cb T 5-MTBE-TOL-30°C b	1.09	24.06	ZSMKZSM-5-MTBE-TOL-30 °Cb T 5-MTBE-TOL-30°C b	1.06	24.35
ZSMKZSM-5-MTBE-TOL-100 °CT 5-MTBE-TOL-100°C	1.05	23.88	ZSMKZSM-5-MTBE-TOL-100 °CT 5-MTBE-TOL-100°C	1.01	23.99
ZSMKZSM-5-MTBE-TOL-400 °CT 5-MTBE-TOL-400°C	0.94	23.72	ZSMKZSM-5-MTBE-TOL-400 °CT 5-MTBE-TOL-400°C	1.00	24.10

Straightstraight channel (K(SC-B)T SC-B)	ε	CFA	Sinu-soidalsinusoidal channel (K(ZZ-B)T ZZ-B)	ε	CFA
ZSMKZSM-5a T 5 a	1.02	22.68	ZSMKZSM-5a T 5 a	1.06	22.65
ZSMKZSM-5-MTBE-DCE-30 °Cb T 5-MTBE-DCE-30°C b	1.04	23.67	ZSMKZSM-5-MTBE-DCE-30 °Cb T 5-MTBE-DCE-30°C b	1.10	23.15
ZSMKZSM-5-MTBE-TOL-30 °Cb T 5-MTBE-TOL-30°C b	1.05	23.59	ZSMKZSM-5-MTBE-DCE-100 °CT 5-MTBE-DCE-100°C	1.07	22.92
			ZSMKZSM-5-MTBE-DCE-400 °CT 5-MTBE-DCE-400°C	1.07	22.81

Straightstraight channel (K(SC-B)T SC-B)	ε	CFA	Sinu-soidalsinusoidal channel (K(ZZ-B)T ZZ-B)	ε	CFA
			ZSMKZSM-5-MTBE-TOL-30 °Cb T 5-MTBE-TOL-30°C b	1.1	22.95
			ZSMKZSM-5-MTBE-TOL-100 °CT 5-MTBE-TOL-100°C	0.93	24.08
			ZSMKZSM-5-MTBE-TOL-400 °CT 5-MTBE-TOL-400°C	1.08	24.23

aRef. 25 .

bRef. 17 .

The C.F.A. values smaller than the maximum value (diameter 7.6 ÅÅ) for an ideal circular 10-ring channel (CFA = 24.5 ÅÅ^2) accounts for the cell volume contraction observed upon heating. Above 500 °C, the unit-cell volume contraction continues until the end of the heat treatment without any mass loss giving rise to a negative thermal expansion (NTE) process (Figures 2 and 3). This phenomenon, already described not only in MFI-zeolites [20,50–52] but also in other microporous materials [53,54], is due to the relaxation in the framework distortions induced by extraframework extra-framework molecules diffusing through the framework during the desorbing stage. [55,56] In summary, Rietveld refinement has evidenced structural modifications of both framework and extraframework extra-framework components. In particular, evolved differently depending on the investigated compound. Additionally, the study of binary systems has evidenced that desorption of single components depends on the mixture composition. Differences in the desorption of MTBE among the two investigated competitive systems (ZSM-5-MTBE-DCE and ZSM-5-MTBE-TOL) is an example of this. To gain information on the host−guest interactions, the adsorption isotherms from aqueous solutions of the three investigated compounds on ZSM-5 were investigated.

To gain information on the host-guest interactions, the adsorption isotherms from aqueous solutions of the three investigated compounds on ZSM-5 were investigated.

3.2. Effects of temperature Temperature on adsorption Adsorption

Adsorption isotherms were measured in dilute aqueous solutions. In Under these conditions, adsorption isotherms are generally linear. The thermodynamic parameters obtained from linear adsorption isotherms measured at different temperatures allow to determine the adsorption enthalpy.

Figure 5. Adsorption isotherms in the low concentration range at four different temperatures (from 5.5 to 23 °C): (a) TOL, (b) MTBE, and (c) DCE.

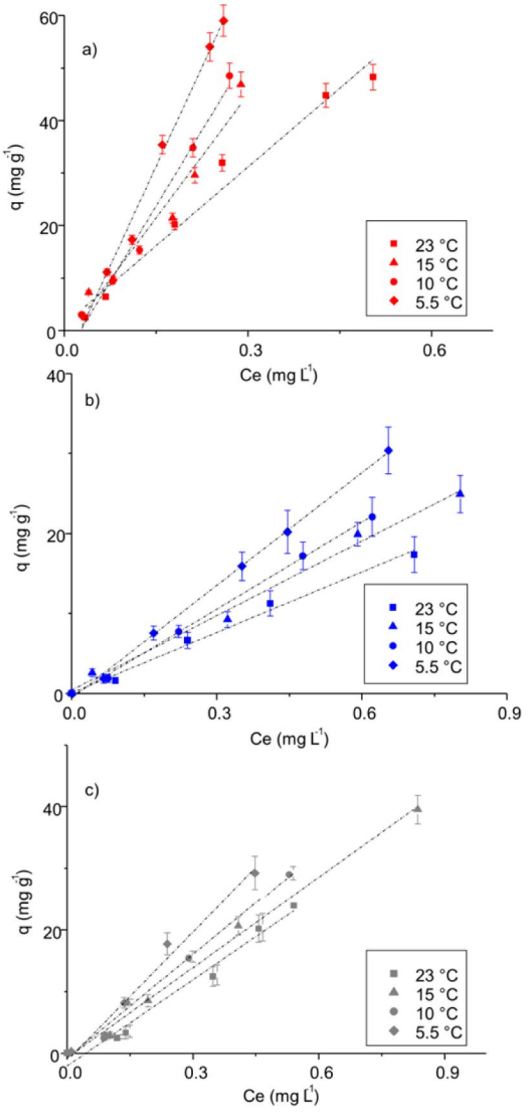

The TOL adsorption isotherms~~,~~ in the low concentration range~~,~~ at four different temperatures (from 5.5 to 23 °C) are reported in Figure 5 a. It is seen that the adsorbed quantity is directly proportional to the solution concentration and the proportionality constant is the adsorption constant of TOL from aqueous solutions. Similar behavior has been observed for the adsorption of diluted aqueous solution of MTBE and DCE (see ~~Figures~~Figure 5 b ~~and ,5~~ c, respectively).

Table 3. Enthalpy ~~change~~Change for ~~toluene~~Toluene, MTBE, and DCE ~~adsorption~~Adsorption onto ZSM-5 from ~~gas~~Gas and ~~aqueous solution.~~Aqueous Solution

	Δ*H* adsorption (gas phase, from literature) (kJ mol^{-1})	Δ*H* adsorption (aqueous solution, experimental) (kJ mol^{-1})	Δ*H* adsorption (gas phase, calculated from eq. 2) (kJ mol^{-1})	Δ*S* adsorption (aqueous solution, calculated from eq. 3) (J mol^{-1} K^{-1})
toluene	−84 [a]	−42	−78	82
	−100 [b]			
	−83 [c]			
	−86 [d]			
MTBE	−90 [e]	−28	−75	72
DCE	−50 [f]	−33	−66	57

[a] Ref. 57.

[b] Ref. 58.

[c] Ref. 59.

[d] Ref. 60.

[e] Ref. 61.

[f] Ref. 62.

The adsorption constant values differ from those measured from gas phase mixture since the measured value takes into account of the interactions in the solution phase and in the adsorbed phase. Additionally, since K_{ads} from aqueous solution at a range of temperatures are available, we can calculate the enthalpy change associated with transfer of TOL to zeolites from aqueous solutions. According to the van't Hoff equation:

$$\ln = -R \qquad (1)$$

where $K_{ads,2}$ and $K_{ads,1}$ are the equilibrium constants at temperatures T_2 and T_1, respectively, ΔH is the enthalpy change for the process, and R is the universal gas constant.

The van't Hoff plot for the ZSM-5-TOL system is shown in Figure 6 a, and by multiplying the slope of the van't Hoff plot and the gas constant, a ΔH value of −42 kJ mol^{-1} for TOL was obtained (see Table 3). Analogously, the enthalpy change for MTBE and DCE, obtained from data plotted in Figure 6 b and 6 c, respectively, were calculated, and the data are reported in Table 3 . The adsorption of all of the three investigated compounds on ZSM-5 is exothermic. Therefore, the adsorption constant decreases with the increasing of system temperature. To compare the experimental data of adsorption enthalpy to that obtained in gas phase system a thermodynamic cycle was considered. The cycle includes: a (1) removal of the organic compound from the aqueous solution, (2) vaporization of the organic compound, and (3) adsorption of the organic compound in gas phase into the zeolite pores. The enthalpy change corresponding to the immersion of the HS zeolite into water was neglected since it is of the order of few mJ mol^{-1} as reported in ref 55. Consequently, the adsorption process of the organic from aqueous solution can be divided up as follows:

$$\Delta H = \Delta H + \Delta H + \Delta H \qquad (2)$$

where $\Delta H_{ads,aq}$ is the enthalpy calculated from the aqueous adsorption isotherms, ΔH_{mix} is the partial molar heat of mixing, and ΔH_{vap} is the heat of vaporization. The enthalpies data available from literature are reported in Table 4 . By substituting the data of Tables 3 and 4 into eq 2 , the calculated adsorption enthalpy from gas phase into ZSM-5 were comparable to those experimentally obtained in previous works (see Table 3). [57,58]

~~is the partial molar heat of mixing, and ΔH_{vap} is the heat of vaporization. The enthalpies data available from literature are reported in Table 4 . By substituting the data of Tables 3 and 4 into eq. 2 the calculated adsorption enthalpy from gas phase into ZSM-5 were comparable to those experimentally obtained in previous works (see Table 3). 57 58~~

Figure 6. van't Hoff plot for the adsorption of: (a) TOL, (b) MTBE, and (c) DCE on ZSM-5.

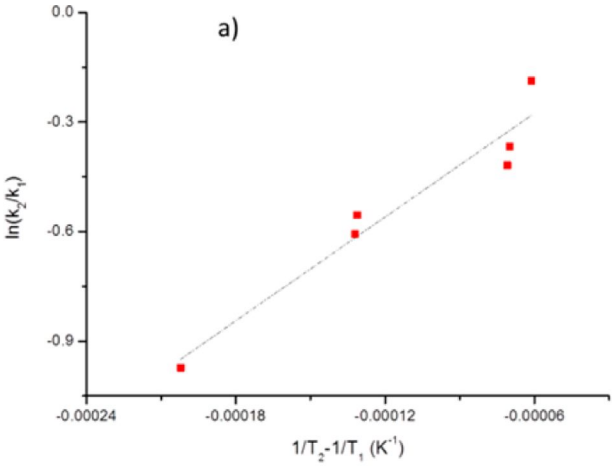

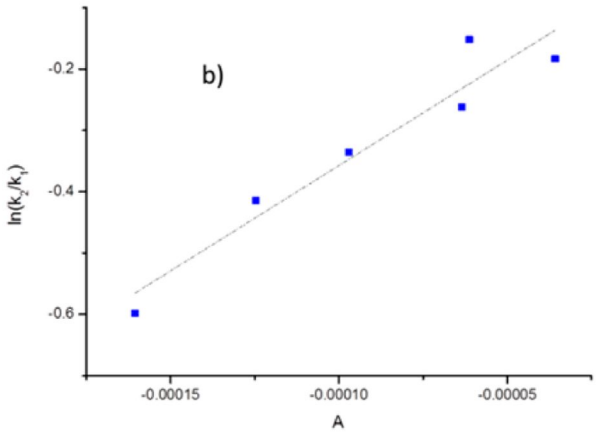

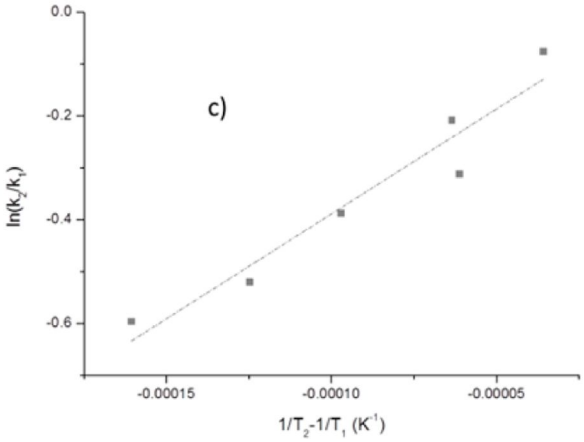

~~Additionally, the process entropy change (ΔS) can be calculated for each temperature by:~~

$$\ln K = \Delta H - T\Delta S \quad (3)$$

Additionally, the process entropy change (ΔS) can be calculated for each temperature by

$$\ln = \Delta - T\Delta \quad (3)$$

The values obtained are −82 and −72, and −57 J mol^{-1} K^{-1} for TOL, MTBE, and DCE, respectively. The negative ΔS indicates that the degrees of freedom of the system decrease during the adsorption process. As a matter of fact, the organic molecules experience a strong confinement within the zeolite micropores due to the framework oxygen interactions. By comparing the adsorption enthalpy of the three investigated compounds, the more strongly adsorbed species is TOL. This finding seems to be in contrast to the order of the sequence of the organics molecules release observed by XRPD Rietveld analysis (see Figure 3). In fact, TOL is released at lower temperature than is DCE possibly indicating a lower binding energy.

Table 4. Physical and chemical properties Chemical Properties of toluene Toluene, MTBE, and DCE.[a]

	MW	Water water solubility (K(g/L)T g/L)	K log K_{ow} T log Kow	T_b (°C)	ΔHH vaporization (K(kJ mol^{-1})T kJ mol^{-1})	ΔHH mixing (K(kJ mol^{-1})T kJ mol^{-1})	ΔHH solvation (K(kJ mol^{-1})T kJ mol^{-1})
Toluene toluene	92.14	0.52	2.77	110.6	−37	11 [b]	−32 [c]
						0.75 [d]	
						1.8 [e]	
MTBE	88.15	48	1.2	55.2	−30	−17 [b]	−49 [c]
						−17 [f]	
DCE	98.95	8.6	1.79	83.5	−35 [g]	2.4 [g]	−33 [g]
					−35 [h]		−28 [c]

[a]Data from NIST Chemistry WebBook when reference is not reported. Data are approximated to two significant digits.

[b]Ref. 63 .

[c]Ref. 64 .

[d]Ref. 65 .

[e]Ref. 66 .

[f]Ref. 67 .

[g]Ref. 68 .

[h]Ref. 62 .

However, this apparent data mismatch is not unusual for MFI zeolite. Indeed, it has already reported a similar behavior for the hexane isomers in MFI zeolite,; in this case too, the more strongly adsorbed species nC6n C6 is more mobile in the structure with respect to the less strongly adsorbed species 2methyl2-methyl pentane. [32,55–,56]

Figure 7. (a) Discrete numerically differentiation of the data of Figure 3 a,. (TOL-) MTBE and TOL (-MTBE) are the differentiation of the of MTBE and TOL occupancies as a function of the temperature of the ZSM-5-TOL-MTBE system, respectively; TOL-MTBE is obtained as a sum of (TOL-) MTBE and TOL (-MTBE), (b) discrete numerically differentiation of the data of Figure 3 b, (DCE-) MTBE and DCE (-MTBE) are the differentiation of MTBE and DCE occupancies as a function of the temperature of the ZSM-5-DCE-MTBE system, respectively; DCE-MTBE is obtained as a sum of (DCE-) MTBE and DCE (-MTBE), (c) DTG curve of ZSM-5-MTBE-TOL, and (d) DTG curve of ZSM-5-MTBE-DCE..

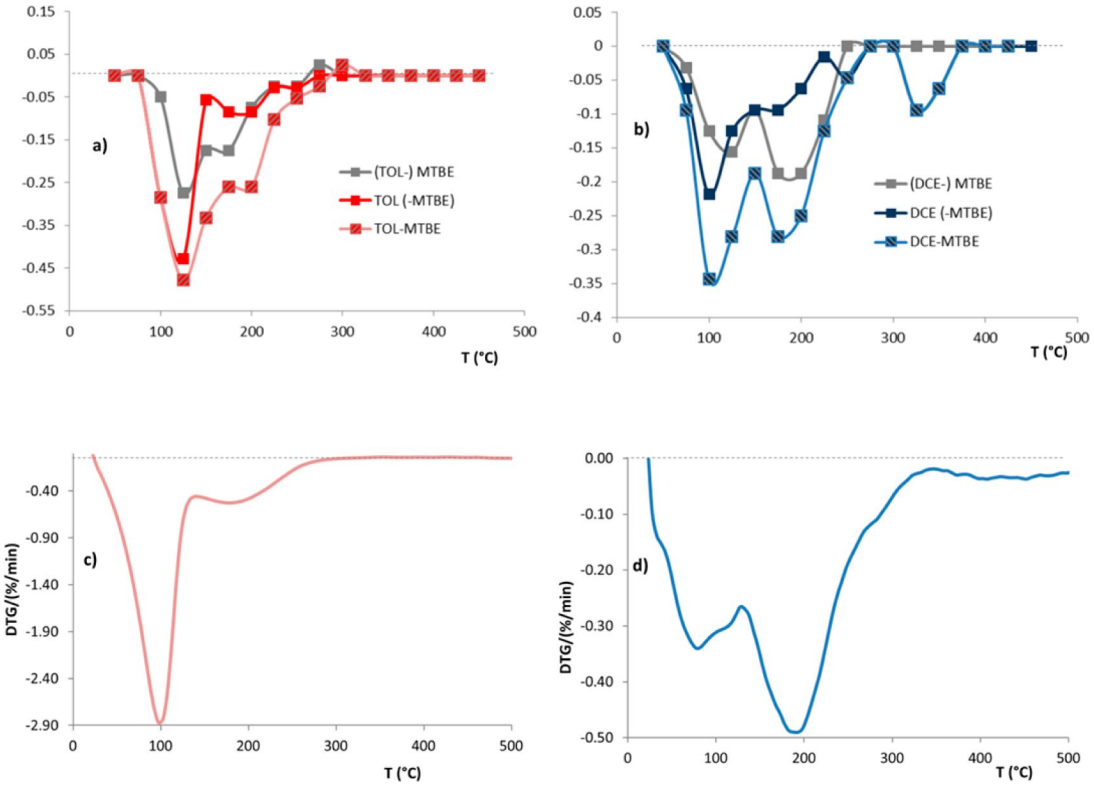

This result confirms that the opposite order between strength of the adsorption interactions and mobility is mainly due to configurational effects of the molecules inside the framework. This hypothesis is further confirmed by comparing the release of DCE from MFI[20] in which it can be seen that the mobility of DCE in the straight channel is higher than that localized close to the intersection. ~~Figures~~Figure 7 a ~~and ,7~~ b ~~show~~shows the discrete numerically differentiation of the data of ~~Figures~~Figure 3 a ~~and ,3~~ b, respectively, obtained from Rietveld refinement of XRPD patterns. These transformed data can be qualitatively employed to enhance differences in the thermal desorption process of a given molecule localized at different positions in the zeolitic ~~extraframework~~extra-framework. Figure 7 also shows DTG curves of the ZSM-5 saturated with binary mixtures (see ~~Figures~~Figure 7 c ~~and ,7~~ d). Strong similarities can been observed between the shape profiles of DTG and the ones obtained as a sum of the differential occupancy data of the two components of the zeolite saturated with binary mixtures (see Figure 7). In particular, by comparing the mass weight loss and the sum of the differential of the refined occupancies of the sites as a function of temperature, it can be seen that at least two peaks are present and that their maxima occur at similar temperature. Additionally, by comparing the differential occupancy of MTBE in the two mixtures (see ~~Figures~~Figure 7 a ~~and ,7~~ b) it can be observed that the second peak of MTBE, is located at higher temperature, and it is more pronounced when the compound is principally adsorbed in the site close to the intersection (i.e., MTBE1 in Figure 1 a) than when it is localized in ZZ channel (i.e., MTBE2 in Figure 1 b). Moreover, from these data it can be inferred that a compound mainly adsorbed in a given site is desorbed in a range of temperature. Therefore, the desorption temperature, seems to be mainly related to position of the molecule inside the porous structure. On the contrary, by comparing the profiles of DCE and TOL in ~~Figures~~Figure 7 a ~~and ,7~~ b, it appears that different compounds having different adsorption enthalpy can be desorbed at similar temperature. This finding is consistent with earlier interpretation of adsorbed molecules at high coverage reported by Sastre et al.[69] and Corma et al.[70] ~~70~~ In conclusion, location of the molecules inside the structure plays an important role the desorption process and it seems critical to estimate the binding energies of the adsorption sites based only on the mass desorbed as a function of temperature.

4. Conclusions

This paper, for the first time, provides detailed information on the thermal desorption behavior of high silica ZSM-5 zeolite loaded with MTBE-DCE and DCE-TOL binary mixtures.

This process was studied in real time using different parallel approaches: (1) macroscopic (i.e., adsorption isotherms) information and (2) microscopic ones (i.e., structural refinements) provided by *in situ* high-temperature (HT) synchrotron X-ray powder diffraction (XRPD). *In situ* high-temperature (HT) synchrotron X-ray powder diffraction (XRPD) allowed us to monitor the evolution of this adsorbent medium during thermal regeneration. A detailed study of the ZSM-5-loaded structure during the heating is presented, including the analysis of the occupancy variations during the temperature-induced-desorption process. The time evolution of the occupancies of MTBE as a function of temperature, in the ZSM-5 saturated with TOL-MTBE and DCE-MTBE mixtures, is different, and it depends on the location of MTBE inside the ZSM-5 structure when adsorbed from the two different binary solutions.[17]

Adsorption enthalpy of the three different compounds do not correlate with desorption suggesting that configurational effects can affect the mobility of the adsorbent molecules inside the framework. The hypothesis was confirmed by the negative ΔS values indicates that the degrees of freedom decrease during the adsorption process. The information obtained from structural refinements was employed for interpretation thermogravimetric analysis. To the best of our knowledge, this is one of the first works showing detailed experimental evidence at microscopic level of the desorption process of binary mixtures. In particular, it gives experimental evidence of the relevance of the location of the compound inside the porous structure on the desorption process.

Supporting Information

The Supporting Information is available free of charge on the ACS Publications website Publications website. Refined atomic coordinates, occupancy factors, thermal parameters at different temperatures DOI: 10.1021/acs.jpcc.7b05090 and the evolution of thermal isotropic displacement factors for the ZSM-5-MTBE-DCE and ZSM-5-TOL-MTBE structures (PDF).

Refined atomic coordinates, occupancy factors, thermal parameters at different temperatures and the evolution of thermal isotropic displacement factors for the ZSM-5-MTBE-DCE and ZSM-5-TOL-MTBE structures (PDF)

Author Contributions

The manuscript was written through contributions of all authors. All authors have given approval to the final version of the manuscript. All authors contributed equally.

Acknowledgments

This study was carried out within a project founded by the SoWaZe PRIN and Grant PRIN 2012ATMNJ 003 programs of the Italian Ministry for University and Research (MIUR), as well as the Laboratory Terra&Acqua Tech, Technopole of Ferrara of Emilia-Romagna High Technology Network. We acknowledge the European Synchrotron Radiation Facility (ESRF, Grenoble) for provision of beamtime to proposal CH-3510 "In situ XRD study of structural modifications and desorption kinetics of zeolites used for removal of non polar organic compounds from contaminated water".

The authors declare no competing financial interest.

ABBREVIATIONS Abbreviations

DCE, 1,2-dichloethane; GC, Gas Chromatography gas chromatography; Hs, Headspace headspace; HS, Hydrophobic hydrophobic/ organophilic high-silica zeolites; HT, high temperature; MTBE, methyl-*tert*-buthyl-ether; NTE, negative thermal expansion; SC, straight channel; MS, Mass Spectrometry mass spectrometry; TG, Thermogravimetry thermogravimetry; DTG, derivative thermogravimetry; TOL, Toluene toluene; XRPD, X-ray powder diffraction; ZSM-5- MTBE- DCE, ZSM-5- methyl-*tert*-buthyl-ether – 1,2-dichloethane; ZSM-5-MTBE-TOL, ZSM-5- methyl-tert-buthyl-ether - Toluene toluene; ZZ, sinusoidal channel

References

(1) Martucci, A.; Braschi, I.; Marchese, L.; Quartieri, S. Recent Advances in Clean-up Strategies of Waters Polluted with Sulfonamide Antibiotics: A Review of Sorbents and Related Properties. *Miner Mineral. Mag.* **2014**, *78*, 1115–1140 10.1180/minmag.2014.078.5.03.

(2) Damjanović, L.; Rakić, V.; Rac, V.; Stošić, D.; Auroux, A. The Investigation of Phenol Removal from Aqueous Solutions by Zeolites as Solid Adsorbents. *J. Hazard. Mater.* **2010**, *184*, 477–484 10.1016/j.jhazmat.2010.08.059.

(3) Datt, A.; Fields, D.; Larsen, S. C. An Experimental and Computational Study of the Loading and Release of Aspirin from Zeolite HY. *J. Phys. Chem. C* **2012**, *116*, 21382–21390 10.1021/jp3067266.

(4) Martucci, A.; Pasti, L.; Marchetti, N.; Cavazzini, A.; Dondi, F.; Alberti, A. Adsorption of Pharmaceuticals from Aqueous Solutions on Synthetic Zeolites. *Micropor. Mesopor. MatMicroporous Mesoporous Mater*. **2012**, *148*, 174–18310.1016/j.micromeso.2011.07.009.
(5) Pasti, L.; Sarti, E.; Cavazzini, A.; Marchetti, N.; Dondi, F.; Martucci, A. Factors Affecting Drug Adsorption on Beta Zeolites. *J. Sep. Sci.* **2013**, *36*, 1604–16110.1002/jssc.201201142.
(6) Martucci, A.; Cremonini, M.AM. A.; Blasioli, S.; Gigli, L.; Gatti, G.; Marchese, L.; Braschi, I. Adsorption and Reaction of Sulfachloropyridazine Sulfonamide Antibiotic on a High Silica Mordenite: A Structural and Spectroscopic Combined Study. *Micropor. Mesopor. MatMicroporous Mesoporous Mater*. **2013**, *170*, 274–28610.1016/j.micromeso.2012.11.031.
(7) Datt, A.; Burns, E.AE. A.; Dhuna, N.AN. A.; Larsen, S.CS. C. Loading and Release of 5 Fluorouracil from HY Zeolites with Varying SiO_2/Al_2O_3 ratios. *Micropor. Mesopor. MatMicroporous Mesoporous Mater*. **2013**, *167*, 182–18710.1016/j.micromeso.2012.09.011.
(8) Amorim, R.; Vilaça, N.; Martinho, O.; Reis, R.MR. M.; Sardo, M.; Rocha, J.; Fonseca, A.MA. M.; Baltazar, F.; Neves, I. C. Zeolite Structures Loading with an Anticancer Compound as Drug Delivery Systems. *J. Phys. Chem. C* **2012**, *116*, 25642–2565010.1021/jp3093868.
(9) Braschi, I.; Blasioli, S.; Gigli, L.; Gessa, C.EC. E.; Alberti, A.; Martucci, A. Removal of Sulfonamide Antibiotics from Water: Evidence of Adsorption into an Organophilic Zeolite Y by its Structural Modifications. *J. Hazard. Mater.* **2010**, *17178*, 218–22510.1016/j.jhazmat.2010.01.066.
(10) Blasioli, S.; Martucci, A.; Paul, G.; Gigli, L.; Cossi, M.; Johnston, C. T.; Marchese, L.; Braschi, I. Removal of Sulfamethoxazole Sulfonamide Antibiotic from Water by High Silica Zeolites: a Study of the Involved Host–guest Interactions by a Combined Structural, Spectroscopic, and Computational Approach. *J. Colloid Interf.Interface Sci.* **2014**, *419*, 148–15910.1016/j.jcis.2013.12.039.
(11) Sarti, E.; Chenet, T.; Pasti, L.; Cavazzini, A.; Rodeghero, E.; Martucci, A. Effect of Silica Alumina Ratio and Thermal Treatment of Beta Zeolites on the Adsorption of Toluene from Aqueous Solutions. *Minerals* **2017**, *7*, 2210.3390/min7020022.
(12) Milestone, N. B.; Bibby, D. M. Concentration of Alcohols by Adsorption on Silicalite. *J. Chem. Technol. BiotBiotechnol.* **1981**, *31*, 732–73610.1002/jctb.280310198.
(13) Yazaydin, A. O.; Thompson, R. W. Molecular Simulation of the Adsorption of MTBE in Silicalite, Mordenite, and Zeolite Beta. *J. Phys. Chem. B* **2006**, *110*, 14458–1446210.1021/jp061986n.
(14) Abu-Lail, L.; Bergendahl, J. A.; Thompson, R. W. Adsorption of Methyl Tertiary Butyl Ether on Granular Zeolites: Batch and Column Studies. *J. Hazard. Mater.* **2010**, *178*, 363–36910.1016/j.jhazmat.2010.01.088.
(15) Anderson, M. A. Removal of MTBE and other Organic Contaminants from Water by Sorption to High Silica Zeolites. *Environ. Sci. Technol.* **2000**, *34*, 725–72710.1021/es990390t.
(16) Rossner, A.; Knappe, D. R. MTBE Adsorption on alternative Adsorbents and Packed Bed Adsorber Performance. *Water Res.* **2008**, *42*, 2287–229910.1016/j.watres.2007.12.009.
(17) Pasti, L.; Rodeghero, E.; Sarti, E.; Bosi, V.; Cavazzini, A.; Bagatin, R.; Martucci, A. Competitive Adsorption of VOCs from Binary Aqueous Mixtures on Zeolite ZSM-5. *RSC Adv.* **2016**, *6*, 54544–5455210.1039/C6RA08872D.
(18) Rodeghero, E.; Martucci, A.; Cruciani, G.; Bagatin, R.; Sarti, E.; Bosi, V.; Pasti, L. Kinetics and Dynamic Behaviour of Toluene Desorption from ZSM-5 using In Situ High-temperature Synchrotron Powder X-Ray Diffraction and Chromatographic Techniques. *Catal. Today* **2016**, *227277*, 118–12510.1016/j.cattod.2015.11.031.
(19) Rodeghero, E.; Pasti, L.; Sarti, E.; Cruciani, G.; Bagatin, R.; Martucci, A. Temperature-Induced Desorption of Methyl tert-Butyl Ether Confined on ZSM-5: An In Situ Synchrotron XRD Powder Diffraction Study. *Minerals* **2017**, *7*, 3410.3390/min7030034.
(20) Martucci, A.; Rodeghero, E.; Pasti, L.; Bosi, V.; Cruciani, G. Adsorption of 1, 2-Dichloroethane on ZSM-5 and Desorption Dynamics by In Situ Synchrotron Powder X-Ray Diffraction. *Micropor. Mesopor. MatMicroporous Mesoporous Mater*. **2015**, *215*, 175–18210.1016/j.micromeso.2015.05.035.
(21) Perego, C.; Bagatin, R.; Tagliabue, M.; Vignola, R. Zeolites and Related Mesoporous Materials for Multi-talented Environmental Solutions. *Micropor. Mesopor. MatMicroporous Mesoporous Mater*. **2013**, *166*, 37–4910.1016/j.micromeso.2012.04.048.
(22) Sacchetto, V.; Gatti, G.; Paul, G.; Braschi, I.; Berlier, G.; Cossi, M.; Marchese, L.; Bagatin, R.; Bisio, C. The Interactions of Methyl tert-Butyl Ether on High Silica Zeolites: a Combined Experimental and Computational Study. *Phys. Chem. Chem. Phys.* **2013**, *15*, 13275–1328710.1039/c3cp51684a.

(23) Arletti, R.; Martucci, A.; Alberti, A.; Pasti, L.; Nassi, M.; Bagatin, R. Location of MTBE and Toluene in the Channel System of the Zeolite Mordenite: Adsorption and Host––Guest Interactions. *J. Solid State Chem.* **2012**, *194*, 135–142 10.1016/j.jssc.2012.04.024.
(24) Martucci, A.; Pasti, L.; Nassi, M.; Alberti, A.; Arletti, R.; Bagatin, R.; Vignola, R.; Sticca, R. Adsorption Mechanism of 1, 2-Dichloroethane into an Organophilic Zeolite Mordenite: a Combined Diffractometric and Gas Chromatographic Study. *Micropor. Mesopor. MatMicroporous Mesoporous Mater.* **2012**, *151*, 358–367 10.1016/j.micromeso.2011.10.010.
(25) Pasti, L.; Martucci, A.; Nassi, M.; Cavazzini, A.; Alberti, A.; Bagatin, R. The Role of Water in DCE Adsorption from Aqueous Solutions Onto Hydrophobic Zeolites. *Micropor. Mesopor. MatMicroporous Mesoporous Mater.* **2012**, *160*, 182–193 10.1016/j.micromeso.2012.05.015.
(26) Braschi, I.; Gatti, G.; Bisio, C.; Berlier, G.; Sacchetto, V.; Cossi, M.; Marchese, L. The Role of Silanols in the Interactions between Methyl tert-Butyl Ether and High-Silica Faujasite Y: an Infrared Spectroscopy and Computational Model Study. *J. Phys. Chem. C* **2012**, *116*, 6943–6952 10.1021/jp210605t.
(27) Leardini, L.; Martucci, A.; Braschi, I.; Blasioli, S.; Quartieri, S. Regeneration of High-Silica Zeolites after Sulfamethoxazole Antibiotic Adsorption: a Combined In-situ High-Temperature Synchrotron X-Ray Powder Diffraction and Thermal Degradation Study. *MinerMineral. Mag.* **2014**, *78*, 1141–1160 10.1180/minmag.2014.078.5.04.
(28) Braschi, I.; Blasioli, S.; Buscaroli, E.; Montecchio, D.; Martucci, A. Physicochemical Regeneration of High Silica Zeolite Y used to Clean-up Water Polluted with Sulfonamide Antibiotics. *J. Environ. Sci.* **2016**, *43*, 302–312 10.1016/j.jes.2015.07.017.
(29) Vignola, R. ; Cova, U. ; Fabiani, F. ; Sbardellati, T. ; Sisto, R. Process for the Regeneration of Non-polar Adsorbing Zeolites used for the Treatment of Contaminated Water. *Patent publication number :* WO, 2009000429 2009, A1.
(30) Kamiya, N.; Iwama, W.; Kudo, T.; Nasuno, T.; Fujiyama, S.; Nishi, K.; Yokomori, Y. Determining the Structure of a Benzene 7. 2-Silicalite-1 Zeolite Using a Single-Crystal X-Ray Method. *Acta Crystallogr., Sect. B: Struct. Sci.* **2011**, *67*, 508–515 10.1107/S0108768111038560.
(31) Fujiyama, S.; Kamiya, N.; Nishi, K.; Yokomori, Y. Reanalysis of CO_2-Silicalite-1 Structure as Monoclinic Twinning. *Z. Kristallogr. - Cryst. Mater.* **2014**, *229*, 303–309 10.1515/zkri-2013-1663.
(32) Krishna, R. Separating Mixtures by Exploiting Molecular Packing Effects in Microporous Materials. *Phys. Chem. Chem. Phys.* **2015**, *17*, 39–59 10.1039/C4CP03939D.
(33) Krishna, R.; van Baten, J. M. Highlighting a Variety of Unusual Characteristics of Adsorption and Diffusion in Microporous Materials Induced by Clustering of Guest Molecules. *Langmuir* **2010**, *26*, 8450–8463 10.1021/la904895y.
(34) Kamiya, N.; Oshiro, T.; Tan, S.; Nishi, K.; Yokomori, Y. Adsorption Process of Phenol on Silicalite-1 and Crystal Structure of Phenol8. 0-Silicalite-1 using a Single Crystal X-Ray Diffraction Method. *Micropor. Mesopor. MatMicroporous Mesoporous Mater.* **2013**, *169*, 168–175 10.1016/j.micromeso.2012.11.006.
(35) Alberti, A.; Martucci, A. Phase Transformations and Structural Modifications Induced by Heating in Microporous Materials. *Stud. Surf. Sci. Catal.* **2005**, *155*, 19–43 10.1016/S0167-2991(05)80135-1.
(36) Alberti, A.; Martucci, A. Reconstructive Phase Transitions in Microporous Materials: Rules and Factors Affecting Them. *Micropor. Mesopor. MatMicroporous Mesoporous Mater.* **2011**, *141*, 192–198 10.1016/j.micromeso.2010.11.014.
(37) Cruciani, G. Zeolites upon Heating: Factors Governing their Thermal Stability and Structural Changes. *J. Phys. Chem. Solids* **2006**, *67*, 1973–1994 10.1016/j.jpcs.2006.05.057.
(38) Polikarpov, M.; Snigireva, I.; Snigirev, A. X-ray harmonics rejection on third-generation synchrotron sources using compound refractive lenses. *J. Synchrotron RadRadiat.* **2014**, *21*, 484–487 10.1107/S1600577514001003.
(39) PANalytical, B. V. *X'Pert HighScore Plus software* X'Pert HighScore Plus software v.3.0e3.0e ,; 2006 , PANalytical, B. V. : Almelo, The Netherlands , 2006 .
(40) Larson, A. C. ; Von Dreele, R. B. *General Structure Analysis System (GSAS)*,; Los Alamos National Laboratory Report LAUR 86––748; Los Alamos National Laboratory Los Alamos, NM , 2000.
(41) Toby, B. H. EXPGUI, a Graphical User Interface for GSAS. *J. Appl. Crystallogr.* **2001**, *34*, 210–213 10.1107/S0021889801002242.
(42) Agostini, G.; Lamberti, C.; Palin, L.; Milanesio, M.; Danilina, N.; Xu, B.; Janousch, M.; van Bokhoven, J. A. In situ XAS and XRPD parametric Rietveld refinement to understand dealumination of Y zeolite catalyst. *J. Am. Chem. Soc.* **2010**, *132*, 667–678 10.1021/ja907696h.

(43) Thompson, P.; Cox, D. E.; Hastings, J. B. Rietveld Refinement of Debye–Scherrer Synchrotron X-Ray Data from Al_2O_3 . *J. Appl. Crystallogr.* **1987**, *20*, 79–8310.1107/S0021889887087090.
(44) Felsche, J.; Luger, S.; Baerlocher, C. Crystal Structures of the Hydro-sodalite $Na_6[AlSiO_4]_6$ $8H_2O$ and of the Anhydrous Sodalite $Na_6[AlSiO_4]_6$. *Zeolites* **1986**, *6*, 367–37210.1016/0144-2449(86)90064-3.
(45) Cruciani, G.; Gualtieri, A. Dehydration Dynamics of Analcime by In Situ Synchrotron Powder Diffraction. *Am. Mineral.* **1999**, *84*, 112–11910.2138/am-1999-1-212.
(46) Seryotkin, Y. V.; Joswig, W.; Bakakin, V. V.; Belitsky, I. A.; Fursenko, B. A. High-Temperature Crystal Structure of Wairakite. *Eur. J. Mineral.* **2003**, *15*, 475–48410.1127/0935-1221/2003/0015-0475.
(47) Leardini, L.; Martucci, A.; Cruciani, G. The unusual Thermal Expansion of Pure Silica Sodalite Probed by In Situ Time-Resolved Synchrotron Powder Diffraction. ~~*Micropor. Mesopor. Mat*~~*Microporous Mesoporous Mater.* **2012**, *151*, 163–17110.1016/j.micromeso.2011.10.042.
(48) Martucci, A.; Rodeghero, E.; Cruciani, G. Continuous Dehydration of Cavansite under Dynamic Conditions: an In Situ Synchrotron Powder-Diffraction Study. *Eur. J. Mineral.* **2016**, *28*, 5–1310.1127/ejm/2015/0027-2512.
(49) Ardit, M.; Martucci, A.; Cruciani, G. Monoclinic–Orthorhombic Phase Transition in ZSM-5 Zeolite: Spontaneous Strain Variation and Thermodynamic Properties. *J. Phys. Chem. C* **2015**, *119*, 7351–735910.1021/acs.jpcc.5b00900.
(50) Leardini, L.; Martucci, A.; Cruciani, G. The unusual Thermal Behaviour of Boron-ZSM-5 Probed by "In situ" Time-resolved Synchrotron Powder Diffraction. ~~*Micropor. Mesopor. Mat*~~*Microporous Mesoporous Mater.* **2013**, *173*, 6–1410.1016/j.micromeso.2013.01.036.
(51) Bhange, D. S.; Ramaswamy, V. Enhanced Negative Thermal Expansion in MFI Molecular Sieves by Varying Framework Composition. ~~*Micropor. Mesopor. Mat*~~*Microporous Mesoporous Mater.* **2010**, *130*, 322–32610.1016/j.micromeso.2009.11.029.
(52) Milanesio, M.; Artioli, G.; Gualtieri, A. F.; Palin, L.; Lamberti, C. Template Burning inside TS-1 and Fe-MFI Molecular Sieves: an In Situ XRPD Study. *J. Am. Chem. Soc.* **2003**, *125*, 14549–14558 10.1021/ja037229+.
(53) Martucci, A.; de Lourdes Guzman-Castillo, M.; Di Renzo, F.; Fajula, F.; Alberti, A. Reversible Channel Deformation of Zeolite Omega during Template Degradation Highlighted by In Situ Time-resolved Synchrotron Powder Diffraction. ~~*Micropor. Mesopor. Mat*~~*Microporous Mesoporous Mater.* **2007**, *104*, 257–26810.1016/j.micromeso.2007.02.040.
(54) Leardini, L.; Martucci, A.; Alberti, A.; Cruciani, G. Template Burning Effects on Stability and Boron Coordination in Boron Levyne Studied by In Situ Time Resolved Synchrotron Powder Diffraction. ~~*Micropor. Mesopor. Mat*~~*Microporous Mesoporous Mater.* **2013**, *167*, 117–12610.1016/j.micromeso.2012.02.013.
(55) Krishna, R. The Maxwell–Stefan Description of Mixture Diffusion in Nanoporous Crystalline Materials. ~~*Micropor. Mesopor. Mat*~~*Microporous Mesoporous Mater.* **2014**, *185*, 30–5010.1016/j.micromeso.2013.10.026.
(56) Malherbe, R. R.; Wendelbo, R. Study of Fourier Transform Infrared-Temperature-Programmed Desorption of Benzene, Toluene and Ethylbenzene from H-ZSM-5 and H-Beta Zeolites. *Thermochim. Acta* **2003**, *400*, 165–17310.1016/S0040-6031(02)00488-4.
(57) Xu, D.; Ma, J.; Zhao, H.; Liu, Z.; Li, R. Adsorption and Diffusion of n-Heptane and Toluene over Mesostructured ZSM-5 Zeolitic Materials with Acidic Sites. *Fluid Phase Equilib.* **2016**, *423*, 8–1610.1016/j.fluid.2016.04.013.
(58) Huang, Q.; Vinh-Thang, H.; Malekian, A.; Eić, M.; Trong-On, D.; Kaliaguine, S. Adsorption of n-Heptane, Toluene and o-Xylene on Mesoporous UL-~~ZSM5 Materials~~ZSM5Materials. ~~*Micropor. Mesopor. Mat*~~*Microporous Mesoporous Mater.* **2006**, *87*, 224–23410.1016/j.micromeso.2005.08.011.
(59) Pope, C. G. Sorption of Benzene, Toluene, and p -Xylene on Silicalite and H-ZSM-5. *J. Phys. Chem.* **1986**, *90*, 835–83710.1021/j100277a025.
(60) Mukti, R. R.; Jentys, A.; Lercher, J. A. Orientation of Alkyl-Substituted Aromatic Molecules during Sorption in the Pores of H/ZSM-5 Zeolites. *J. Phys. Chem. C* **2007**, *111*, 3973–398010.1021/jp066715r.
(61) Güvenç, E.; ~~Göktuğ~~ Ahunbay, M. G. Adsorption of Methyl Tertiary Butyl Ether and Trichloroethylene in MFI-Type Zeolites. *J. Phys. Chem. C* **2012**, *116*, 21836–2184310.1021/jp3067052.
(62) Simonot-Grange, M.-H.; Garrot, B. Thermodynamics and Kinetics of Adsorption of Gaseous Single Cl/Br-VOCs of the Ethane Series onto Siliceous ZSM-5 at 25 °C. Prediction of the Adsorption Selectivity in the Gas Phase. *Langmuir* **2001**, *17*, 8188–819210.1021/la0109011.

(63) Atik, Z.; Gruber, D.; Krummen, M.; Gmehling, J. Measurement of Activity Coefficients at Infinite Dilution of Benzene, Toluene, Ethanol, Esters, Ketones, and Ethers at Various Temperatures in Water Using the Dilutor Technique. *J. Chem. Eng. Data* **2004**, *49*, 1429–1432 10.1021/je049875+.
(64) Mintz, C.; Clark, M.; Acree, W. E., Jr.; Abraham, M. H. Enthalpy of Solvation Correlations for Gaseous Solutes Dissolved in Water and in 1-Octanol Based on the Abraham Model. *J. Chem. Inf. Model.* **2007**, *47*, 115–121 10.1021/ci600402n.
(65) Neely, B. J.; Wagner, J.; Robinson, R. L., Jr.; Gasem, K. A. M. Mutual Solubility Measurements of Hydrocarbon–−Water Systems Containing Benzene, Toluene, and 3-Methylpentane. *J. Chem. Eng. Data* **2008**, *53*, 165–174 10.1021/je700449z.
(66) De Lisi, R.; Goffredi, M.; ~~Turco~~ Liveri, V. T. Calorimetric Determination of Solution Enthalpies of Liquids with a Small Mutual Solubility at 298.15 K. *J. Chem. Soc., Faraday Trans. 1* **1980**, *76*, 1660–1662 10.1039/f19807601660.
(67) Nielsen, T. B.; Hvidt, S.; Keiding, S. R.; Petersen, C.; Westh, P.; Keiding, K. Thermodynamic Investigations of Methyl tert-Butyl Ether and Water Mixtures. *Phys. Chem. Chem. Phys.* **2011**, *13*, 1182–1188 10.1039/C0CP00494D.
(68) Hallèn, D. Enthalpies of Solution and Heat Capacities for Some α,ω-Dichloroalkanes in Water. *J. Chem. Thermodyn.* **1993**, *25*, 519–524 10.1006/jcht.1993.1160.
(69) Sastre, G.; Raj, N.; Catlow, C. R. A.; Roque-Malherbe, R.; Corma, A. Selective Diffusion of C8 Aromatics in a 10 and 12 MR Zeolite. A Molecular Dynamics Study. *J. Phys. Chem. B* **1998**, *102*, 3198–3209 10.1021/jp980053r.
(70) Corma, A.; Catlow, C. R. A.; Sastre, G. Diffusion of Linear and Branched C7 Paraffins in ITQ-1 Zeolite. A Molecular Dynamics Study. *J. Phys. Chem. B* **1998**, *102*, 7085–7090 10.1021/jp9813084.